Proceedings of the 21st ICSMGE, Vienna, Austria, 14 – 19 June 2026. Pistrol, Adam & Schweiger (eds.)
Published by: ÖGG, Austrian Society for Geomechanics, Salzburg, Austria, ISBN 978-3-9503898-4-5
https://doi.org/10.53243/ICSMGE2026-2390

Centrifuge test and FEA on uplift resistance of multi-belled piles in dense sand with surface pressure

Yoshihiro Horii, Kentaro Hama, Toru Watanabe
Technology Center, Taisei Corporation, Yokohama, Japan, horii@arch.taisei.co.jp

C F Leung, S C Chian
Civil and Environmental Engineering, National University of Singapore, Singapore

ABSTRACT: Recently in Japan, large-diameter, cast-in-place concrete multi-belled piles have been increasingly used to support greater building load and seismic forces. However, there is still lack of understanding on evaluation of uplift resistance of such piles in deep soils, particularly for piles with bell upper inclination angles exceeding 12°. A detailed study using centrifuge model tests and finite element (FE) analyses using the Mohr - Coulomb criterion in Abaqus were conducted. In the centrifuge tests, double-belled model piles were embedded in dense sand under a surcharge pressure of 200 kPa. The bell spacing ratio, L_t/D_{p3}, was varied from 5 to 18, while the depth of the middle bell was held constant. Results showed that the pile head load at a normalized displacement of $\delta_0 = 0.1\ D_3$ (δ_0: pile head displacement, D_3: end bell diameter), denoted as $P_{0,0.1}$, did not vary significantly for $10 \leq L_t/D_{p3} \leq 18$. However, for $L_t/D_{p3} = 5$, the average load was approximately 20 % lower compared to the range $10 \leq L_t/D_{p3} \leq 18$. Additionally, the ratio of the shared load of the end bell per annular horizontal projection area when $\delta_b/D_3 = 0.1$ (δ_b: pile end displacement) and the effective vertical pressure of soil, or $q_{b0.1}/\sigma_v'$ was observed to decrease with lower L_t/D_{p3} when $L_t/D_{p3} \leq 10$ but remained constant for $L_t/D_{p3} > 10$. This behavior is attributed to a reduction in the mean principal stress σ_m above the end bell when bell spacing is smaller. With respect to the failure mechanism, the failure began with upward, oblique, expansive push-in failures of the middle and end bells ("*I″*, " *II″*) when L_t/D_{p3} was large. This was followed by shear failure linking the outer edges of the bells (" *III″*), the progression of the initial failure ("*IV″*), and eventually shear failure near the pile shaft (" *V″*). For smaller L_t/D_{p3}, the " *II″* failure mode was less distinct, and " *III″* was observed to occur before " *I″*.

KEYWORDS: Multi-belled piles, uplift resistance, centrifuge model tests, FEA.

1 INTRODUCTION

Recently in Japan, large-diameter, cast-in-place concrete multi-belled piles have been increasingly applied to super-tall buildings to accommodate greater building load and seismic forces (Hama, 2019; Hama, 2021). As a case study, Hama (2023) reported a double-belled pile with a 5.3 m bell diameter, an upper inclination angle of approximately 20°, and a lower end depth of around 50 m embedded in dense sandy soil.

Regarding the uplift behavior of belled piles, Dickin and Leung (1992) conducted centrifuge model tests on single-belled piles. Hirai et al. (2008) carried out in-situ pull-out tests on full-scale multi-belled piles featuring an upper inclination angle of 12°, a diameter of 1.7 m and a length of 23.2 m in sandy ground. Honda et al. (2011) performed discrete element (DE) analyses and proposed a method for estimating uplift capacity of both single- and double-belled piles with 12° bell angles in dense sand. Additionally, Hossein (2017) conducted small-scale model tests of such piles in loose sand.

However, a comprehensive method for evaluating uplift resistance in deep soils, particularly enlarged portions with upper inclination angles greater than 12°, remains underdeveloped. This paper aims to investigate the uplift behavior of double-belled piles with steep bell angles in dense sand and ground surface pressure through centrifuge model tests and finite element analyses (FEA). Special focus is given to the influence of bell spacing on uplift resistance and failure mechanisms.

2 CENTRIFUGE MODEL STUDY

2.1 *Outline of tests*

The uplift behavior of multi-belled piles in sand is influenced by the shape, spacing and depth of the bells and soil density. Centrifuge model testing provides a reliable method for comparative studies, allowing simulation of stress-dependent and nonlinear soil behavior under realistic scaling conditions.

The tests were conducted using the beam-type centrifuge at Taisei Corporation which has an effective radius of 2.65 m (Nagura et al., 1994). A centrifugal acceleration of 50 *g* was applied to 1/50 scale model (where *g* denotes gravitational acceleration).

Figure 1 illustrates the test setup, and Table 1 lists the geometric parameters of the model piles. The test container was a rigid box measuring 700 mm (*L*) × 400 mm (*W*) × 700 mm (*H*). Teflon sheets coated with grease were attached to the inner walls to minimize side friction. Three double-belled piles made of aluminum tubes with a tube thickness of 3 mm and bells affixed to the shaft were installed in dry dense sand. The pile ends were closed.

Each pile had a shaft diameter (D_1) of 20 mm and middle and bell diameter (D_2 and D_3) of 36 mm, representing 1.0 m and 1.8 m at full-scale, respectively. The upper inclination angle of the middle bell was 21°, while the lower angle was 45°, while the end bell had the same upper inclination angle of 21° but with a flat base, replicating the geometry and stiffness of actual non-displacement bored piles.

Table 2 lists the model piles used in the tests. The primary test variable was the bell spacing ratio, L_t/D_{p3} (where L_t is bell spacing and D_{p3} is the protrusion width of the end bell beyond the shaft, as illustrated in Figure 1). While the middle bell depth (L_m) was fixed at 229 mm ($L_m/D_2 = 6.4$), L_t/D_{p3} was varied from 5 to 18 by adjusting the total embedded pile length (L_p) between 290 mm and 388 mm. To ensure reproducibility, tests were repeated for $L_t/D_{p3} = 5, 14$.

Strain gauges were installed inside the pile shafts to measure axial forces. Toyoura sand was attached to the pile surfaces (excluding the upper shaft portion). Steel plates were placed atop the sand to apply uniform surface pressure of 200 kPa under 50 *g* loading. A rubber plate was inserted between the steel plates and soil surface to minimize constraint on soil deformation.

Dry Toyoura sand was used, and its properties are summarized in Table 3. The air-pluviated sand was poured to achieve a relative density (D_r) of approximately 90 % was achieved. Table 4 presents mechanical properties of the dense sand. The effective vertical stress (σ_v') at the location of the middle and end bells was 381 kPa and 484 kPa, respectively.

Before the loading tests, several cycles of centrifuge loading and unloading were performed to minimize soil settlement and reduce negative friction acting on the piles. Once 50 g was applied and soil had fully settled, vertical uplift load were applied to the pile heads using an electric jack. The loading rate was maintained at 0.3 mm/min or slower until the pile head displacement (δ_0) exceeded 0.2 D_3. Intermediate unloading and reloading steps were conducted at δ_0 = 0.01 D_3, and 0.03 D_3 to examine load-displacement behavior.

During centrifuge acceleration, the pile heads were not fixed to the jacking system, allowing them to settle freely with the surrounding soil. Measurements included pile head load, displacement at pile head and soil surface, and axial strain of the piles.

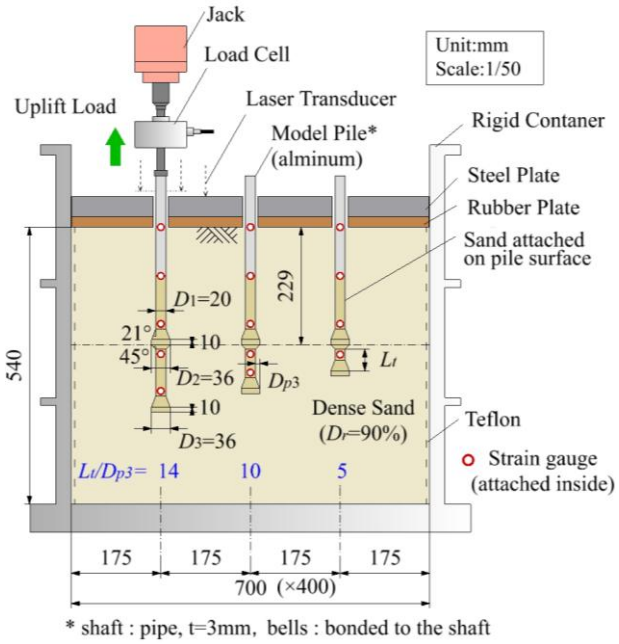

Figure 1. Centrifuge model setup.

Table 1. Parameters of shape for model piles.

Parameter	Symbol	Value	Unit
Shaft diameter	D_1	20	mm
Middle and end bell diameter	D_2, D_3	36	Mm
Upper inclination angle of bell	θ_u	21	°
Lower inclination angle of bell	θ_l	45	°
One-sided protrusion width of middle bell and end one	D_{p2}, D_{p3}	8	mm
Height of bell's maximum diameter	h	10	mm

Table 2. List of model piles.

Bell spacing	Ratio of bell spacing, L_t/D_{p3}	Pile length from soil surfaces, L_p		Num. of tests
		Value	Unit	
Very large	18	388	mm	1
Large	14	360	mm	2
Middle	10	324	mm	1
Small	5	290	mm	2

Table 3. Properties of Toyoura sand.

Parameter	Symbol	Value	Unit
Soil particle density	G_s	2.65	g/cm^3
Maximum dry density	$\rho_{d\,max}$	1.64	g/cm^3
Minimum dry density	$\rho_{d\,min}$	1.36	g/cm^3
Maximum void ratio	e_{max}	0.949	-
Minimum void ratio	e_{min}	0.616	-

Table 4. Properties of dense sand.

Parameter	Symbol	Value	Unit
Relative density (target)	D_r	90	%
Dry density	ρ_d	1.61	g/cm^3
Void ratio	e	0.644	-
Unit weight	γ_s	15.8	kN/m^3

2.2 *Test results*

The test results are discussed here in terms of model scale. All loads and axial forces were recoeded after applying centrifugal acceleration, while displacements were reset to zero at the start of the pull-out tests. Consequently, the measured loads and axial forces include the effect of negative skin friction developed during centrifugal loading. No significant deformation of the soil surface was observed in post-test observations.

Figure 2 presents the relationship between pile head load (P_0) and pile head displacement (δ_0). For all piles, P_0 increased with δ_0 up to a point; however, beyond $\delta_0 > 0.2\ D_3$ (= 7.2 mm), the increase in P_0 became negligible. Table 5 summarizes the pile head load at δ_0 = 0.1 D_3, denoted as $P_{0,0.1}$, which represents the limit resistance in practice. For bell spacing ratio (L_t/D_{p3}) ranging from 10 to 18, $P_{0,0.1}$ showed no significant variation. In contrast, the average $P_{0,0.1}$ for L_t/D_{p3} = 5 was approximately 20% lower than those for $10 \leq L_t/D_{p3} \leq 18$.

Figure 3 illustrates the relationship between the middle bell load (P_m) and its displacement (δ_m), as well as end bell load (P_b) and its displacement (δ_b). The value of P_m was derived from the axial force difference measured by strain gauges placed above and below the middle bell, while P_b was obtained directly from the axial force measured just above the end bell. For larger bell spacing ratios (L_t/D_{p3} = 14 or 18), P_b increased consistently with δ_b, similar to the trend observed for P_m. However, for smaller bell spacing ratiosn(L_t/D_{p3} = 10 or 5), P_b began to decrease once δ_b exceeded 0.1 D_3, and its magnitude was lower than that of P_m.

Table 5 also includes the values of P_b when δ_b = 0.1 D_3 (denoted $P_{b0.1}$) and P_m at δ_m = 0.1 D_2 (denoted $P_{m0.1}$), along with the end and middle bell load per annular horizontal projection area($q_{b0.1}$ and $q_{m0.1}$, respectively). It was observed that $P_{b0.1}$ decreased with L_t/D_{p3} for $L_t/D_{p3} \leq 10$.

Figure 4 illustrates the relationship between the normalized load on the end bell—defined as the ratio of the

shared load per annular horizontal projection area at δ_b/D_3 = 0.1 ($q_{b0.1}$) to the effective vertical stress at the pile end (σ_v') , i.e., $q_{b0.1}/\sigma_v$', and the bell spacing ratio (L_t/D_{p3}). The value of $q_{b0.1}/\sigma_v$' decreased with L_t/D_{p3} when $L_t/D_{p3} \leq 10$, while it remained approximately constant for $L_t/D_{p3} > 10$. Specifically, for L_t/D_{p3} = 5, $q_{b0.1}/\sigma_v$' was about 60% of the average value observed for L_t/D_{p3} >10.

The soil failure mechanisms between bells—later examined in the finite element (FE) analysis—are conceptually illustrated in Figure 5. For large L_t/D_{p3} values, the failure mode likely corresponds to an expansive push-in failure, where a wedge-shaped mass of soil above the end bell moves upward. In contrast, for smaller L_t/D_{p3} values, the failure mode appears to resemble a cylindrical shear failure surface connecting the outer edge of the bells.

Figure 6 presents the relationship between the calculated average shear stress on the assumed cylindrical failure surface at δ_b/D_3 = 0.1 (denoted as $\tau_{s0.1}$)$\tau_{s0.1}$, and L_t/D_{p3}. The results indicate that $\tau_{s0.1}$ remained constant when $L_t/D_{p3} \leq 10$.

The relationship between L_t/D_{p3} and $q_{b0.1}/\sigma_v$' derived from the average shear stress ($\tau_{s0.1ave,}$ see Figure 6) and the area of the assumed cylindrical shear surface closely matched the experimental trend shown in Figure 4. This correspondence supports the interpretation that a cylindrical shear failure mechanism governs uplift resistance when L_t/D_{p3} is small.

Table 5. List of loads at pile head bells.

L_t/D_{p3}	$P_{0,0.1}$ (kN)	$P_{m0.1}$ (kN)	$q_{m0.1}$ (kPa)	$P_{b0.1}$ (kN)	$q_{b0.1}$ (kPa)
5	9.60	5.61	7.98	2.67	3.79
	10.7	6.13	8.72	3.09	4.39
10	11.5	5.76	8.18	4.50	6.39
14	13.1	5.10	7.25	4.99	7.09
	13.4	5.10	7.25	5.07	7.20
18	12.4	4.66	6.62	5.29	7.52

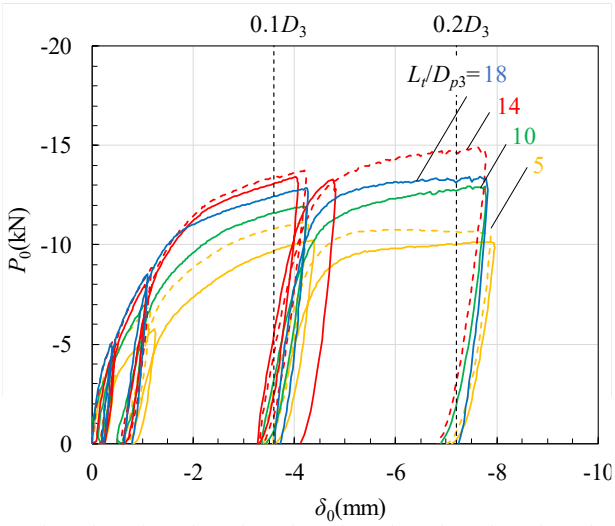

Figure 2. Relationship between pile head load and displacement.

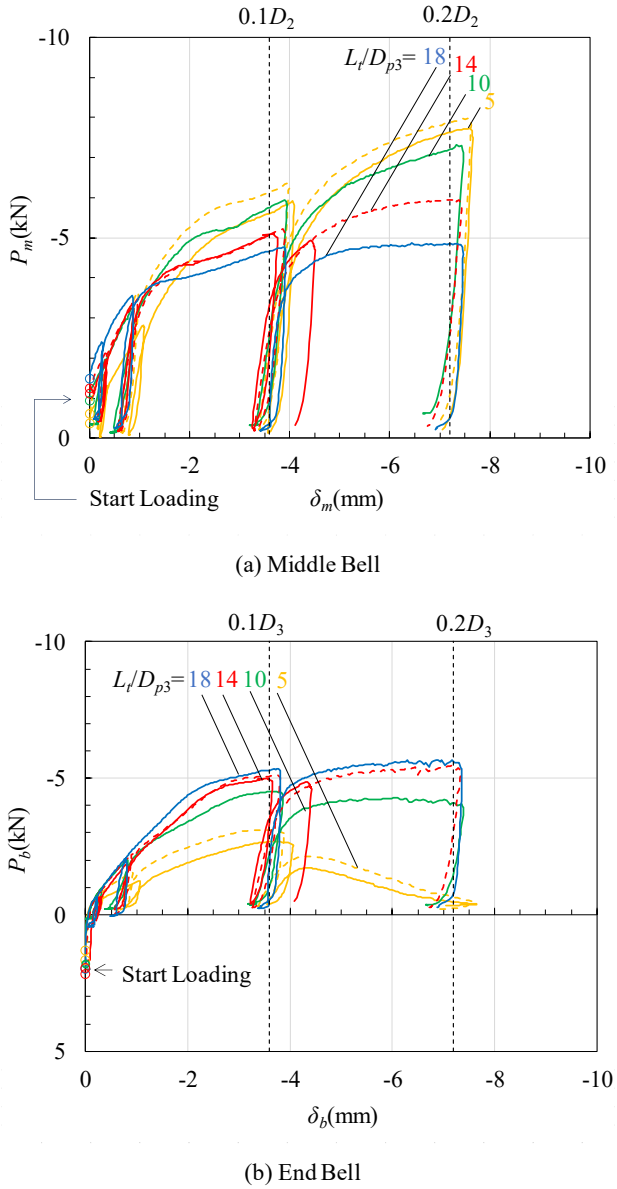

Figure 3. Relationship between load of bells and displacement.

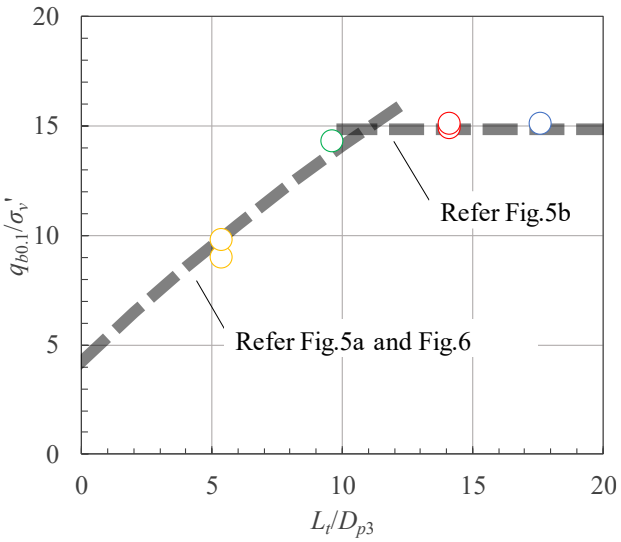

Figure 4. Relationship between $q_{b0.1}/\sigma_v$' and L_t/D_{p3}.

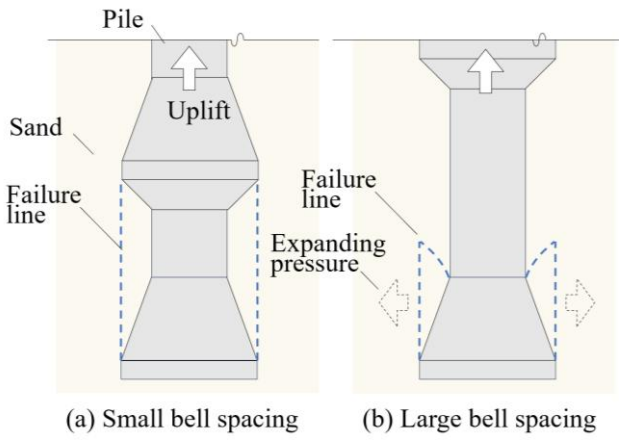

Figure 5. Consideration of soil failure mechanisms between bells.

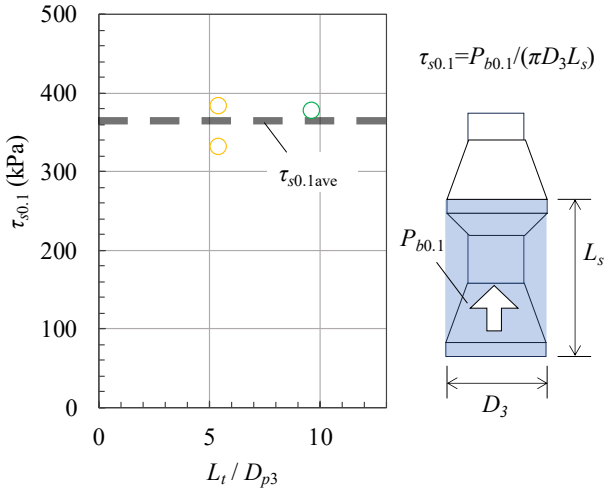

Figure 6. Relationship between $\tau_{s0.1}$ and L_t/D_{p3}.

3 FE ANALYSIS

3.1 *Outline of FEA*

In the centrifuge model tests described earlier, no observable soil deformation beneath the surface was detected. Therefore, finite element (FE) analysis was conducted to further investigate the uplift behavior of multi-belled piles in dense sand. The simulations were performed using Abaqus/Explicit (Simullia 2022). Figure 7 presents the full-scale FE model. The mesh consisted of axisymmetric four-node linear quadrilateral elements (CAX4R). The element width varied from $D_2/40$ to $D_2/2$, where D_2 is the diameter of the middle bell (equal to D_3, the end bell diameter).

The Mohr–Coulomb yield criterion was adopted for the soil, and the plastic potential was defined by a smooth elliptic function that approximates the Mohr–Coulomb failure envelope. The interaction between the pile and the soil accounted for contact, separation, friction and slip. The shear friction stress (τ_f) was calculated using the following equation:

$$\tau_f = \alpha \sigma_n \tan \varphi_s \quad (1)$$

where α is the interface friction coefficient (set to 0.5 in this study), σ_n is the normal stress acting on the pile surface, and φ_s is the shear resistance angle of the soil.

The pile was modeled as an elastic material. Table 6 and Table 7 summarize the physical properties used for the soil and the pile, respectively. Based on preliminary calibration, the soil parameters were set as follows: elastic modulus (E_s) = 300 MN/m^2, internal friction angle (φ_s) = 40°, dilatancy angle (ψ_s) = 0°, cohesion (c_s) = 0, initial static earth pressure coefficient (K_0) = 0.5, unit weight (γ_s) = 16 kN/m^3, and Poisson's ratio (v_s) = 0.3.

Four simulation cases were conducted with bell spacing ratio (L_t/D_{p3}) of 5, 10, 14, and 18. Following the application of self-weight and surface pressure, an upward displacement was applied to pile head until pile head displacement ratio, (δ_0/D_2) reached 0.2.

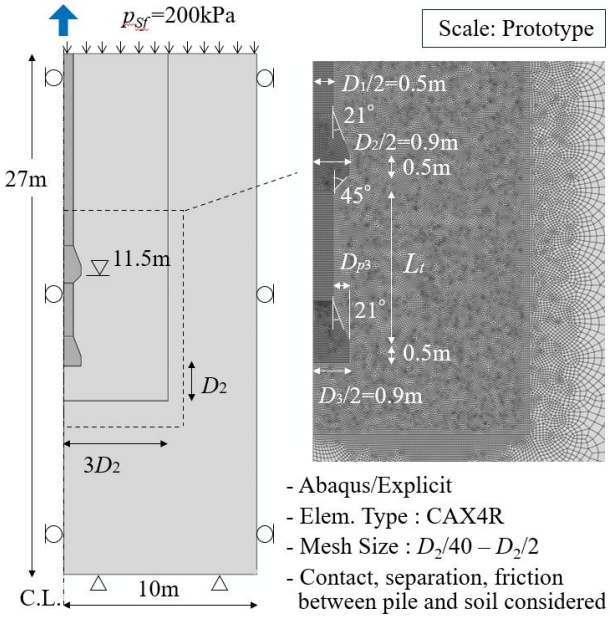

Figure 7. FE Model.

Table 6. Properties of soil used in FEA.

Parameter	Symbol	Value	Unit
Internal friction angle	φ_s	40	°
Dilatancy angle	ψ_s	0	°
Cohesion	c_s	0	kN/m^2
Elastic modulus	E_s	300	MN/m^2
Poisson's ratio	v_s	0.3	-
Unit Weight	γ_s	16	kN/m^3
Initial static earth pressure coefficient	K_0	0.5	-

Table 7. Properties of pile used in FEA.

Parameter	Symbol	Value	Unit
Young's modulus	E_p	36,000	MN/m^2
Poisson's ratio	v_p	0.3	°
Unit Weight	γ_p	16	kN/m^3

3.2 *Results of FEA*

The analysis results are discussed in the model scale, consistent with experimental data, using the initial value from the onset of loading.

Figure 8 compares the finite element analysis (FEA) results with the centrifuge test results for the relationship between the load (P_0) and the displacement ratio (δ_0/D_2). In the FEA, P_0 increased with both δ_0/D_2 and the bell spacing ratio (L_t/D_{p3}). The FEA results generally agreed with the test results when $\delta/D_2 \leq 0.1$. However, for $\delta/D_2 > 0.15$, the FEA tended to overestimate the pile head load. This discrepancy is likely due to the FEA not accounting for the reduction in the

internal friction angle (φ_s) of dense sand under increasing strain.

Figure 9 shows the shared load of the middle and the end one at $\delta_0/D_2 = 0.1$, denoted $P_{m0.1}$ and $P_{b0.1}$ respectively, plotted against L_t/D_{p3}, comparing FEA and test results. The FEA successfully reproduced the observed trend: $P_{b0.1}$ decreased with decreasing L_t/D_{p3}, while the $P_{m0.1}$ remained approximately constant.

Figure 10 presents the mean principal stress of soil (σ_m) at $\delta/D_2 = 0.1$ for cases with L_t/D_{p3} =5 and 14. The results show that σ_m in the region above the end bell was significantly lower for L_t/D_{p3} =5 compared to L_t/D_{p3} =14. This stress reduction is considered a key factor contributing to the lower $P_{b0.1}$ observed at smaller bell spacing ratios.

Figure 11 illustrates the soil displacement vector fields for two cases (L_t/D_{p3} =5 and 14). The displacement was generally directed upward between the bells and obliquely upward above the middle bell. Notably, the displacements did not reach the soil surface—consistent with the centrifuge test observations, indicating that the middle bell was embedded deeply. In fact, the depth ratio of the middle bell (L_m/D_2) was as high as 6.4, and a surcharge pressure of 200 kPa was applied.

Figure 12 shows the distribution of accumulated plastic shear strain of soil (ξ), which is used to represent soil failure. The incremental plastic shear strain was calculated using the following expression:

$$\Delta\xi = \sqrt{\frac{2}{3}\{(\Delta\varepsilon_1 - \Delta\varepsilon_2)^2 + (\Delta\varepsilon_2 - \Delta\varepsilon_3)^2 + (\Delta\varepsilon_3 - \Delta\varepsilon_1)^2\}} \quad (2)$$

where $\Delta\varepsilon_1$, $\Delta\varepsilon_2$ and $\Delta\varepsilon_3$ are incremental principal plastic strains during each step of the calculation.

In the case with a large bell spacing (L_t/D_{p3} =14), the mean stress below the bells decreased, and initial uplift loading caused expansive push-in failures directed obliquely upward from both the middle bell ("*I*") and the end bell ("*II*"). This was followed by shear failure linking the outer edge of the bells ("*III*") , continued upward progression of the push-in failure above the middle bell ("*IV*"), and finally shear failure in the vicinity of the shaft ("*V*"). In contrast, for the case with small bell spacing (L_t/D_{p3} =5), failure mode ("*II*") was less distinct, and the one between bells ("*III*") occurred before the push-in failure ("*I*"). Soil failure generally did not extend to the ground surface, except near the shaft.

Although the FEA model did not capture all aspects of strain-softening behavior in dense sand, particularly the reduction in φ_s, the results reasonably reproduced the uplift behavior and failure mechanisms of multi-belled piles in dense sand under surface pressure within this experimental range.

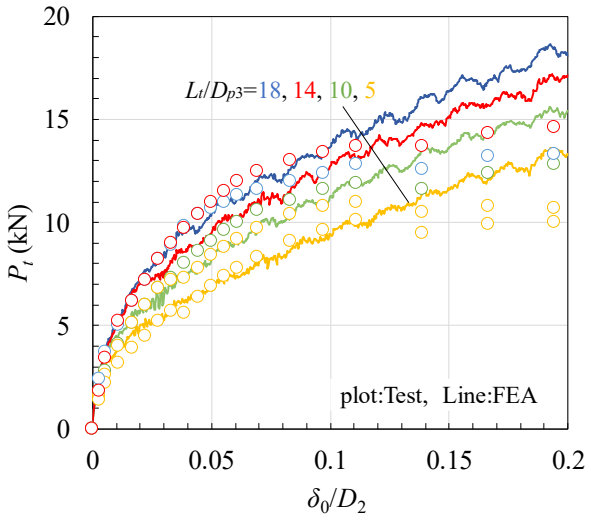

Figure 8. FE result of load-displacement relationship at pile head.

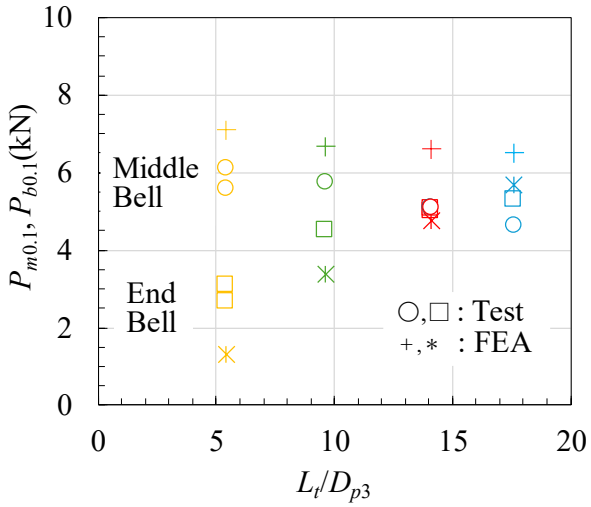

Figure 9. FE result of shared load of bells when δ_0/D_2=0.1

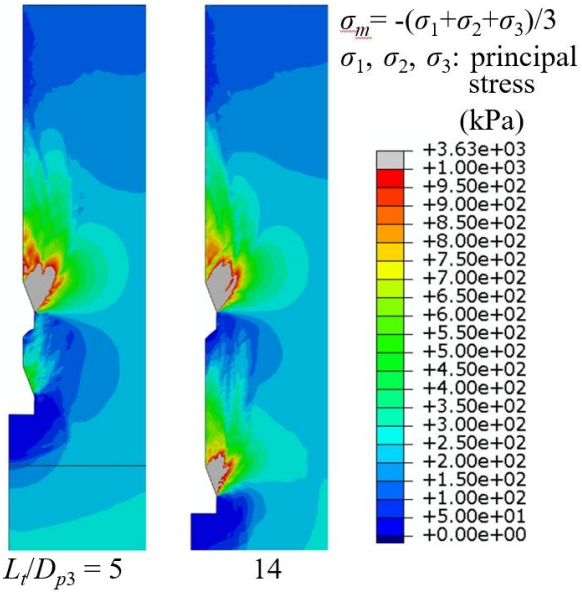

Figure 10. FE result of mean principal stress of soil when δ_0/D_2=0.1.

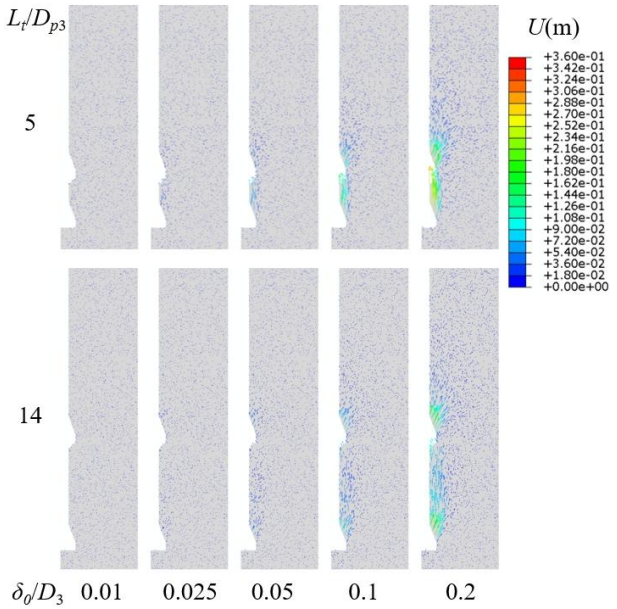

Figure 11. FE result of soil displacement vector.

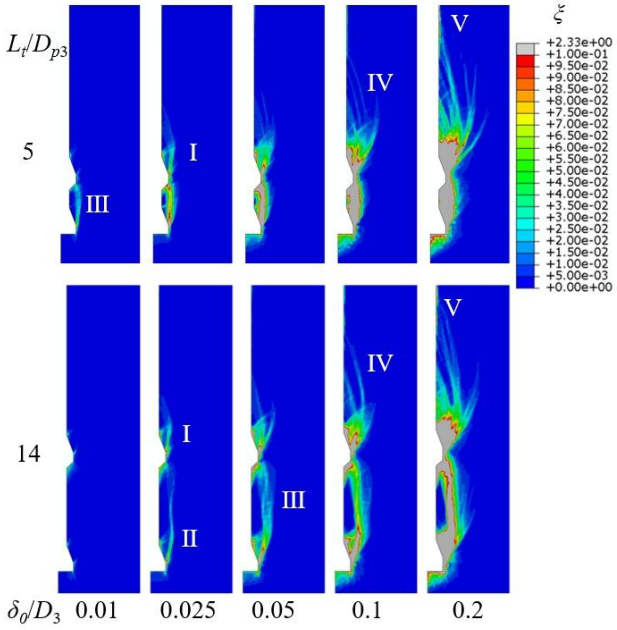

Figure 12. FE result of soil failure, ξ, contour.

4 CONCLUSIONS

In this study, the uplift resistance and failure mechanisms of multi-belled piles embedded in a dense sand under the surface pressure of 200 kPa were investigated through centrifuge model tests and finite element (FE) analyses. The centrifuge tests employed double-belled piles with a shaft diameter (D_1) of 20 mm, middle and end bell diameters (D_2, D_3) of 36 mm. The upper inclination angles of the bells was 21°, and a scale factor of 1/50 was used under a centrifugal acceleration of 50 *g*. The bell spacing ratio (L_t/D_{p3}, where L_t was bell spacing and D_{p3} was protrusion width of the end bell relative to the shaft) was varied from 5 to 18, while the depth ratio of the middle bell (L_m/D_2) was kept constant at 6.4. Based on the results of the experimental and numerical analyses, the following conclusions were drawn:

- The pile head load (P_0) increased with pile head displacement (δ_0), but exhibited limited growth beyond $\delta_0 > 0.2\ D_3$.
- Pile head load at $\delta_0 = 0.1\ D_3$ ($P_{0.0.1}$), which represents to the limit resistance in practice, showed little variation within the range $10 \leq L_t/D_{p3} \leq 18$. However, for $L_t/D_{p3} = 5$, the average of $P_{0.0.1}$ is approximately 20 % lower than the one for larger spacing ratios.
- The ratio of end bell load per annular horizontal projection area at $\delta_b/D_3 = 0.1$ to effective vertical stress at the pile end ($q_{b0.1}/\sigma_v'$) decreased with L_t/D_{p3} for $L_t/D_{p3} \leq 10$, but remained nearly constant for $L_t/D_{p3} > 10$. This reduction is attributed to a drop in the mean principal stress (σ_m) above the end bell for smaller spacing ratios.
- Finite element results using Mohr–Coulomb failure criterion (Abaqus/Explicit) revealed that, when L_t/D_{p3} is large, the mean stress below the bells decreases, initiating expansive push-in failures directed obliquely upward from both the middle bell ("*I*") and end bell ("*II*"). This is followed by shear failure connecting the outer edges of the bells ("*III*"), upward progression of the push-in failure above the middle bell ("*IV*"), and finally shear failure near the pile shaft ("*V*"). In contrast, for small bell spacing ratios ($L_t/D_{p3} = 5$), failure mode "*II*" becomes indistinct, and the shear failure between bells ("*III*") tends to precede the push-in failure ("*I*").

5 ACKNOWLEDGEMENTS

The centrifuge model tests described in Chapter 2 were conducted in collaborations with System Measure Co., Ltd. The authors gratefully acknowledge the company's significant support and contributions to this study.

6 REFERENCES

Dickin, E. A., Leung C. F. 1992. The influence of foundation geometry on the uplift behaviour of piles with enlarged bases. *Canadian Geotechnical Journal* 29, 498-505

Hirai, Y., and Aoki, M. 2008. In-situ pull-out tests on uplift resistance behavior of cast-in-place concrete pile with bell enlargement. *Journal of structural engineering*. 54 B, 59-66.

Hama, K., Horii, Y., Nakanishi, Y. and Watanabe, T. 2019. Field trials of large-diameter multi-belled pilling method. *Proc. 4th GEOTEC HANOI 2019*, Hanoi, 161–168.

Hama, K., Watanabe, T., Horii, Y., Akizuki M., Iwata A., Nakanishi, Y., Takuya O., and Mukai Y. 2021. Quality verification from field trials of multi-belled cast-in-place pile using belling bucket without hydraulic drive. *AIJ journal of technology and design* 27(67), 1219-1224.

Hama, K., Watanabe, T., Horii, Y., Toyama, J., Kimura, Y., Akizuki, M., and Nakanishi, Y. 2023. Practical Case of Constructing "T-EAGLE" Pile in Super High-rise Building, *Taisei advanced center of technology technical report*. [Online] Available at: https://www.taisei.co.jp/tact/tr/2023/24/ [Accessed 10th June 2025].

Honda, T., Hirai, and Y., Sato, E. 2011. Uplift capacity of belled and multi-belled piles in dense sand, *Soils and foundations* 51(3), 483−496.

Hossein, M., Mansour, M. 2017. Uplift resistance of belled and multi-belled piles in loose sand, *Measurement* 109, 346-353

Hu, P., Wang, D., Stanier S. A., and Cassidy M. J. 2015. the punch-through hazard of a spudcan on sand overlying clay. *Géotechnique* 65(11), 883–896

Nagura, K., Tanaka, M., Kawasaki, K., and Higuchi, Y. 1994. Development of an earthquake simulator for the TAISEI centrifuge. *Proc. Centrifuge 94*, 151-156.

Simullia. 2022. *ABAQUS manual*. Japan.